Appl. Phys. B 63, 191–197 (1996)

Applied Physics B Lasers and Optics

Photoacoustic soot sensor for in-situ black carbon monitoring

A. Petzold[1], **R. Niessner**[2]

[1] Deutsche Forschungsanstalt für Luft- und Raumfahrt (DLR) Institut für physik der Atmosphäre Oberpfaffenhofen, D-82234 Wessling, Germany
(Fax: + 49-8153/28-1841)
[2] Institute of Hydrochemistry, Technical University of Munich, Marchioninistrasse 17, D-81377 Munich, Germany
(Fax: + 49-89/7095-7999)

Received: 3 November 1995/Accepted: 26 February 1996

Abstract. The PhotoAcoustic Soot Sensor (PASS) for in situ black carbon mass monitoring is presented. The sensor combines a high-power laser diode ($\lambda = 802$ nm; $P = 450$ mW) and a novel spectrophone setup to achieve a portable sensor system for black carbon measurements. The acoustic resonator with a Q-factor of ≈ 300 is operated in its 2nd azimuthal mode at 6670 Hz. To estimate the effects of the window position, laser beam collimation, and different loss mechanisms on spectrophone sensitivity a model treating these effects with respect to the signal strength of the azimuthal modes is described. It gives a cell constant of 5.8 V/(W m^{-1}) in good agreement with 5.9 V/(W m^{-1}) obtained from measurements with particulate carbon. Additionally, this model permits a method for an absolute calibration of the spectrophone. To improve the signal-to-noise ratio, the photoacoustic signal is estimated by a weighted least-squares fit to an averaged line profile of the excited normal mode instead of a direct measurement of peak height. Finally, the application of this data processing algorithm yields a detection limit of 1.5×10^{-6} m^{-1} or 0.5 µg black carbon per m^3

PACS: 07.60; 43.20.Ks; 43.85

Black Carbon (BC) is the dominant absorber of light in the atmospheric aerosol with a featureless absorption spectrum in the VISible (VIS) and Near-InfraRed (NIR) [1]. Common optical methods for BC-monitoring [2–5] are based on the analysis of particle-loaden filter samples for the light-absorbing content of deposited material. As a consequence of analyzing particles deposited on a diffusely reflective filter matrix, a modification of optical properties of the particles compared to their airborne state may occur and cause an incorrect BC measure [6, 7].

These problems in BC determination are avoided by the use of an in-situ absorption measurement technique as photoacoustic spectroscopy [8–10]. To obtain a high selectivity for particulate BC, the spectrophone has to be operated in a spectral range where almost no interfering gases occur (VIS, NIR), or the contributions of absorbing gases, first of all CO_2 and H_2O, have to be derived from a differential measurement and subtracted from the total photoacoustic signal [8, 11]. In this context the recent availability of small-sized high-power laser diodes emitting in the NIR offered the possibility to develop a portable sensor system which will be applicable to field measurements without any effort [12, 13].

Starting with the pioneer work of Terhune and Anderson [14], almost all spectrophones designed for aerosol absorption measurements in the VIS/NIR used a cylindrical azimuthal resonator. But, up to now no theoretical description of such an azimuthal resonant cavity is available which includes effects of laser beam collimation, window position and particle-related relaxational losses on the cell constant of the resonator. The importance of such a theoretical description is evident with respect to a possible absolute calibration of a photoacoustic cell in the absence of NIR-absorbing test gases of known absorbance.

1 Cell constant of a cylindrical resonant chamber

1.1 Basic relations

To achieve sufficient performance characteristics and, above all, to permit an absolute calibration of a photoacoustic spectrophone the effects of acoustic losses as well as position and degree of collimation of the laser beam on the cell constant of a resonant cavity have to be examined. Up to now, results with regard to these questions are available only for radial resonators [15–17] or as general expressions for a complex mode structure [18]. Possible effects of particle-related losses are neglected almost completely.

Starting with a cylindrical cavity of length L and radius R the normal acoustic modes p_j of such a resonator are described by [8, 18]

$$p_j(r, \varphi, z) = p_j J_m\left(\frac{\pi \alpha_{mn}}{R} r\right) \cos(m\varphi) \cos\left(\frac{\pi n_z}{L} z\right), \quad (1)$$

where r, φ, z are standard cylindrical coordinates, $j = (mnn_z)$ and m, n, n_z are the order of azimuthal, radial, and longitudinal mode, respectively, p_j is a normalization coefficient such that $V_c^{-1} \int p_j^* p_k \, dV = \delta_{jk}$ with chamber volume V_c and p_j^* as the complex conjugate of p_j, J_m is the Bessel function of order m, and α_{mn} is the n-th solution of $(dJ_m/dr) = 0$ at $r = R$. The eigenfrequencies of the resonator are given by [8, 18]

$$f_j = \frac{c_0}{2} \sqrt{\left(\frac{\alpha_{mn}}{R}\right)^2 + \left(\frac{n_z}{L}\right)^2}, \tag{2}$$

where c_0 is the speed of sound. In the case of azimuthal mode excitation (n, $n_z = 0$), the resonance frequency reduces to $f_j = c_0 \alpha_{m0} (2R)^{-1}$.

In real systems, dissipation processes cause a broadening of the resonance profile of the acoustic mode in the frequency domain. The symmetric line profile $A(f)$ of such a resonance subjected to acoustic losses can be described by a Lorentzian profile [17] of the form

$$A(f) = A_j f \left[\left(\frac{f \Delta f_j}{(f_j^2 - f^2)^2 + f^2 \Delta f_j^2} \right)^2 + \left(\frac{f_j^2 - f^2}{(f_j^2 - f^2)^2 + f^2 \Delta f_j^2} \right)^2 \right]^{1/2}, \tag{3}$$

where f and f_j are modulation frequency and resonance frequency of mode j, respectively, and Δf_j is the FWHM of the resonance. The quality factor Q_j of mode j is given by the relation $Q_j = f_j / \Delta f_j$. Its reciprocal Q_j^{-1} is a measure for the loss of acoustic energy with respect to the energy stored in mode j.

According to [9] an upper limit for the induced pressure amplitude p_j at beam power P and absorbance β can be expressed as

$$p_j(\omega_j) = \frac{(\gamma - 1) Q_j}{\omega_j} \beta \frac{PL}{V_c} P_j J_m\left(\frac{\pi \alpha_{mn}}{R} r\right), \tag{4}$$

where γ is the ratio of specific heats c_p/c_v at constant pressure and volume. The factor PL/V_c presumes that the coupling between the spatial profile of beam intensity I_b and excited normal mode p_j is ideal [9].

To get a more detailed insight into the efficiency of normal mode excitation the coupling integral between the laser beam and normal mode has to be evaluated. For this purpose, the spatial distribution of the beam intensity may be approximated by a Gaussian distribution [15, 16]

$$I_b(r, \varphi) = \frac{P}{\pi R_b^2} \exp\left\{ - \frac{(r \cos\varphi - R_w)^2 + r^2 \sin^2 \varphi}{R_b^2} \right\}, \tag{5}$$

where R_b is the beam radius and R_w is the position of the laser entrance window. The spatial intensity distribution (5) is normalized such that the integration over the chamber cross-sectional area yields total beam power P regardless of the degree of collimation or window position. In general, $R_w = 0$ holds for the excitation of radial modes and $R_w > 0$ for the excitation of azimuthal modes.

The coupling integral $F(I_b, p_j)$ between the laser beam and normal mode can be written as [8]

$$F(I_b, p_j) = \frac{1}{V_c} \int_{V_c} I_b(r, \varphi) p_j^*(r, \varphi) \, dV. \tag{6}$$

Assuming the spatial profile I_b identical to the excited normal mode, i.e., $I_b \sim P p_j$, it reduces to $F(I_b, p_j) = PL/V_c$, as mentioned above [8, 9, 16]. Otherwise, a correction factor K_j has to be taken into account such that $F(I_b, p_j) = K_j PL/V_c$ with $K_j < 1$ for non-ideal coupling.

Introducing the correction factor K_j into (4), the induced pressure amplitude at resonance frequency $\omega_j = 2\pi f_j$ and at spatial position ($r = R$, $\varphi = 0°$) is given by

$$p_j = \frac{1}{2} \frac{(\gamma - 1) Q_j}{\omega_j} \frac{\beta P}{\pi R^2} K_j P_j J_m(\pi \alpha_{mn}). \tag{7}$$

The factor $\frac{1}{2}$ originates from the fact, that the beam intensity I_b is sinusoidally modulated. Thus, mean absorbed power is only $\frac{1}{2}$ of the unmodulated beam power P [16].

Finally, the cell constant C_c of a resonant cavity, which corresponds to the induced signal (in μV) per unit laser power P and unit absorbance β, may be given as

$$C_c = \frac{1}{2} \frac{(\gamma - 1) Q_j}{\omega_j} \frac{1}{\pi R^2} K_j P_j J_m(\pi \alpha_{mn}) S_{\text{micro}}, \tag{8}$$

where S_{micro} is the sensitivity of the microphone (in μV/Pa). In the following, the factors $P_j J_m(\pi \alpha_{mn})$, Q_j, and K_j will be discussed with special consideration of the azimuthal mode excitation.

1.2 Normalization coefficients and quality factors

As mentioned above, the normalization coefficient P_j is defined such that

$$\frac{1}{V_c} \int_{V_c} p_i^* p_j \, dV = \begin{cases} 1, & i = j, \\ 0, & i \neq j, \end{cases} \tag{9}$$

i.e., the equation

$$\int_{V_c} |p_j|^2 \, dV = \frac{1}{|P_j|^2} \pi R^2 L \tag{10}$$

has to be solved for a given mode j. The results for azimuthal and radial modes are summarized in Table 1. They were calculated from values in [19] using the integral relations of bessel functions.

To estimate the quality factor Q_j of a given mode j, the following loss mechanisms were taken into account: (i) free space viscous and thermal dissipation, (ii) free space dissipation by particle-related thermal relaxation processes, (iii) viscous and thermal losses in the cell boundary layer,

Table 1. Normalization coefficient P_j and factor $P_j J_m(\pi \alpha_{mn})$ for azimuthal modes (m00) and radial modes (0n0), respectively, in a cylindrical cavity

Mode	P_j	$P_j J_m[\pi \alpha_{mn}]$
(m00)	$J_m^{-1}(\pi \alpha_{m0}) \sqrt{2} \left[1 - \left(\frac{m}{\pi \alpha_{m0}} \right)^2 \right]^{-1/2}$	(100) 1.68 (200) 1.87 (300) 2.02
(0n0)	$\frac{1}{J_0(\pi \alpha_{0n})}$	1

and (iv) energy absorption by the microphone [15, 19]. For the calculation of Q-values we used functions p'_j which were not normalized, i.e., $p_j = P_j p'_j$. This is allowed because Q-values are given as a quotient of integral expressions containing functions p_j. Thus, normalization constants cancel.

Starting with the common expressions [15–19] for acoustic losses the contributions of loss mechanisms (i)–(iv) to acoustic energy dissipation may be given in a slightly modified form as:

(i) free space losses

$$\left[\frac{1}{Q_j}\right]_{\text{vol}} = \frac{\omega_j}{c_0}[l_\mu + (\gamma - 1)\, l_\kappa] \tag{11}$$

with characteristic lengths

$$l_\mu = \frac{4}{3}\frac{\mu}{\rho c_0}, \quad l_k = \frac{\kappa}{\rho c_p c_0}, \tag{12}$$

related to thermal conductivity κ and viscosity μ, ρ being the density of gas (for air at standard conditions l_κ and l_μ are of the order of 5×10^{-8} m [19]);

(ii) losses by particle-related thermal relaxation processes as discussed in the following;

(iii) viscous surface losses

$$\left[\frac{1}{Q_j}\right]_\mu = \frac{1}{2}\left(\frac{c_0}{\omega_j}\right)^2 d_\mu \frac{\int |\nabla_t p'_j|^2 \, \mathrm{d}S}{\int |p'_j|^2 \, \mathrm{d}V} \tag{13}$$

with thickness

$$d_\mu = \sqrt{\frac{2\mu}{\rho\omega}} \simeq 2.1 \times 10^{-3} \frac{1}{\sqrt{f}} m \tag{14}$$

and thermal surface losses

$$\left[\frac{1}{Q_j}\right]_\kappa = \frac{1}{2}(\gamma - 1) d_\kappa \frac{\int |p'_j|^2 \, \mathrm{d}S}{\int |p'_j|^2 \, \mathrm{d}V} \tag{15}$$

with thickness

$$d_\kappa = \sqrt{\frac{2\kappa}{\rho c_p \omega}} \simeq 2.5 \times 10^{-3} \frac{1}{\sqrt{f}} m; \tag{16}$$

the effect of surface roughness may be approximated by adding the rms roughness value d_{rms} to thickness d_μ of the viscous boundary layer d_μ [18];

(iv) microphone losses

$$\left[\frac{1}{Q_j}\right]_{\text{micro}} = \frac{1}{2\pi}\frac{A_{\text{micro}}}{S_c}, \tag{17}$$

where A_{micro} and S_c are the surface area of the microphone opening and the inner cell wall, respectively [9]. Power loss through the cell wall and openings in the resonator wall need not be considered if the openings are placed at the nodal points of excited normal modes [18].

To estimate the contribution of particle-related losses due to thermal relaxation processes, a model proposed by Da Silva [20] for molecular relaxational processes is modified to describe particle-related relaxational losses. Starting with the thermal relaxation time

$$\tau = \left(\frac{D_p}{2}\right)^2 \frac{\rho_{\text{part}}\, c_{\text{part}}}{3\kappa} \tag{18}$$

for a particle of diameter D_p, density ρ_{part}, and specific heat capacity c_{part} as reported by Chan [21], we follow the model of Da Silva: viewing a heated particle surrounded by a gas of temperature T as a simple two-level system. If the particles are heated by a laser beam with its intensity varying as a sinusoidal function of time with angular modulation frequency ω, the absorbed energy introduces an excess heat source term

$$\Delta e_{\text{part}}(\tau) = \frac{\rho\, c_{\text{part}}\, T}{1 + \mathrm{i}\omega\tau} \tag{19}$$

to the system. The heated particles reach their final temperature within $t = \tau$, and thus, if $\omega\tau \ll 1$, this temperature is reached throughout each modulation cycle of the radiation. According to [20], the excess heat source Δe_{part} results in a particle-related relaxational loss

$$\left[\frac{1}{Q_j}\right]_{\text{rel}} = \omega_j \left[(\gamma - 1)\,\tau \frac{c_{\text{part}}}{c_p}\right]. \tag{20}$$

This estimate for particle-related losses exhibits all desired properties: losses decrease with decreasing particle diameter D_p and for very large particles with $\omega\tau \gg 1$ excess heat Δe_{part} vanishes and energy loss by relaxation suppresses an efficient excitation of the acoustic normal modes.

In general, $\mathrm{d}V$ and $\mathrm{d}S$ denote integration over chamber volume and chamber surface area, respectively, and ∇_t are the components of the gradient tangential to the area of integration. Using the integral values summarized in Table 2, the following expressions are achieved for surface losses in the case of excited azimuthal

Table 2. Integrals used for the evaluation of surface losses according to (13) and (15)

	$(m00)$	$(0n0)$
$\int \lvert p_j\rvert^2 \, \mathrm{d}V$	$\frac{1}{2}\pi R^2 L\left[1 - \left(\frac{m}{\pi\alpha_{m0}}\right)^2\right] J_m^2(\pi\alpha_{0n})$	$\pi R^2 L J_0^2(\pi\alpha_{0n})$
$\int \lvert p_j\rvert^2 \, \mathrm{d}S$	$\pi R^2 L\left\{\frac{1}{R} + \frac{1}{L}\left[1 - \left(\frac{m}{\pi\alpha_{m0}}\right)^2\right]\right\} J_m^2(\pi\alpha_{m0})$	$2\pi R(R + L)\, J_0^2(\pi\alpha_{0n})$
$\int \lvert \nabla_t p_j\rvert^2 \, \mathrm{d}S$	$2\pi\left[m^2\left(\frac{L}{2R} - 1\right) + (\pi\alpha_{m0})^2 - m\right] J_m^2(\pi\alpha_{m0})$	$2\pi(\pi\alpha_{0n})^2\, J_0^2(\pi\alpha_{0n})$

modes ($m00$)

$$\left[\frac{1}{Q_j}\right]_\mu = 2\frac{d_\mu}{L}\frac{1+(m/\pi\alpha_{m0})^2\,((L/2R)-1)-[m/(\pi\alpha_{m0})^2]}{1-(m/\pi\alpha_{m0})^2}, \tag{21}$$

$$\left[\frac{1}{Q_j}\right]_\kappa = (\gamma-1)d_\kappa\frac{\frac{1}{R}+\frac{1}{L}[1-(m/\pi\alpha_{m0})^2]}{1-(m/\pi\alpha_{m0})^2}, \tag{22}$$

and radial modes ($0n0$)

$$\left[\frac{1}{Q_j}\right]_\mu = \frac{d_\mu}{L} \tag{23}$$

$$\left[\frac{1}{Q_j}\right]_\kappa = (\gamma-1)d_\kappa\frac{1}{L}\left(1+\frac{L}{R}\right). \tag{24}$$

The expressions for radial modes which were calculated as a proof of correctness correspond to those given in [17]. General expressions for modes (mnn_z) are given in [18], but to calculate the integrals for azimuthal modes ($m00$) it is not possible to set $n=0$ and $n_z=0$ and use expressions given in [18] without any modification. The reason for this is that integration over $\cos^2(k_z z)\mathrm{d}z$ with $k_z=\pi n_z/L$ along the cylinder axis yields results $L/2$ for $n_z\neq 0$ and L for $n_z=0$, and this factor is not included in the expressions given in [18]. This can be seen, too, by direct comparison of (21) solved for $m=0$ and (23) for radial mode excitation. Additionally, differences occurred in the expressions containing the integral $\int|\nabla_t p_j'|^2\,\mathrm{d}S$, because in [18] only the azimuthal component of $\nabla_t p_j$ was taken into account for integration over the front surfaces of the cylinder. But, even for pure azimuthal modes the radial velocity $\nabla_t p_j$ does not vanish. This is a straightforward result from calculating ∇p_j with p_j given by (1).

Finally, the quality factor Q_j is obtained by summing over the above-mentioned contributions Q_{ij}^{-1} according to $Q_j^{-1}=\sum Q_{ij}^{-1}$. With that, all the parameters necessary to calculate the cell constant C_c according to (8) are available except S_{micro} which has to be derived from experiment.

2 Experimental

Figure 1 shows a schematic diagram of the sensor setup. The spectrophone is driven by an AlGaAs laser diode (SONY SLD-303) with optical output $P=0.5\,\mathrm{W}$ at an emission wavelength $\lambda=0.802\,\mu\mathrm{m}$. The resonator is of cylindrical shape with diameter $2R=5\,\mathrm{cm}$ and total length $L=10\,\mathrm{cm}$. It is operated in its azimuthal modes (off-axis excitation) with a sample flow of 1.2 l/min. Two electret microphones (SENNHEISER KE 4-211-2) are mounted flush with the inner cell wall at positions of maximum pressure variation in the case of the 2nd azimuthal mode excitation. Measuring the differential signal between both microphones, a doubling of the signal strength of the 2nd azimuthal mode is achieved. According to (8), this signal enhancement almost completely compensates the decrease of cell constant C_c with respect to the higher resonance frequency of the 2nd azimuthal mode ($f_{200}\approx 6700\,\mathrm{Hz}$) compared with the 1st azimuthal

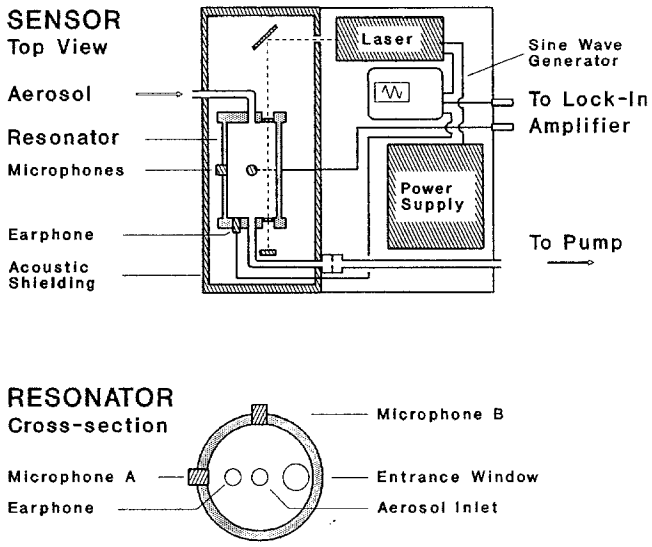

Fig. 1. Schematic diagram of the sensor setup and microphone positions

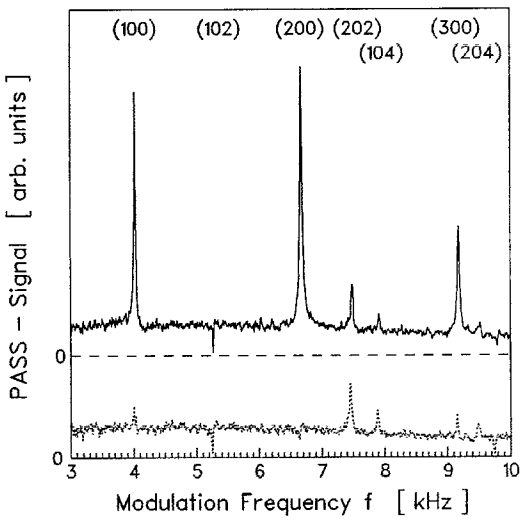

Fig. 2. Acoustic spectrum of the resonator obtained for a differential microphone configuration at constant BC concentration (*solid line*) and for particle-free air (*dotted line*); the orders (mnn_z) of the excited acoustic modes are indicated

mode ($f_{100}\approx 4060\,\mathrm{Hz}$). This effect is demonstrated in Fig. 2 which shows the acoustic spectrum of the resonator in the frequency range 3–10 kHz. The plotted background signal was obtained with particle-free air and corresponds to window heating.

Additionally, an earphone (SENNHEISER KDH 2-1) is placed at one end plate of the cylinder opposite to the entrance window providing an acoustic test-signal to check microphones or resonator characteristics. System control and signal processing are performed with a dual phase lock-in amplifier (HMS DYNATRAC 500) combined with a low noise differential preamplifier (ITHACO Model 568). Further details of the spectrophone setup and optical layout are given elsewhere [12, 13].

3 Data processing

To gain further improvement of the sensor features, a novel data processing algorithm was developed which determines the photoacoustic signal at a given BC mass concentration from estimation of the peak height by weighted least-squares fit to a resonance profile instead of a direct measurement of the peak height. According to (3), the resonance profile of an excited mode in the frequency domain is assumed to be of a Lorentzian line shape. For each measurement six frequency scans over the resonance are averaged. The fitted resonance profile is obtained by a Marquardt-Levenberg algorithm [22] which yields mean signal strength and standard deviation as a function of modulation frequency f. A similar approach was proposed by Poston and Harris [23] for photoacoustic measurements in the time domain.

To increase the number of samples for the determination of an average line profile above $n = 6$ is not recommended for F values and Student's t values do not change significantly beyond this point. On the other hand, time resolution deteriorates with increasing n. In the algorithm described here, averaging over $n = 6$ scans takes 1 min, the frequency resolution of the scans is about 2.5 Hz, and measuring frequencies range about $\pm$ 75 Hz with respect to the resonance frequency f_j of the excited mode. Thus, complete detection of a mode with $Q \geq 250$ and $f_j \approx 6700$ Hz is guaranteed.

The time constant τ_c of the resonator, i.e., the time for the signal to equal $1 - e^{-1}$ of its final value, was calculated (volume divided by flow) from a sample flow of 1.2 l/min and a sample cell volume of 196 cm^3 to be $\approx$ 16 s. Estimating the time required to produce full response to a constant BC concentration, a time resolution of 80 s is achieved if $t = 5\tau_c$ is assumed to be long enough for a complete exchange of sample gas in the cell. This time resolution is in satisfactory agreement with the duration of the averaging procedure. Hence, no information about temporal variations of BC concentration is lost by applying the outlined data processing algorithm to BC mass monitoring.

4 Results and discussion

4.1 *Efficiency of mode excitation*

The efficiency of mode excitation by a laser beam of Gaussian intensity distribution may be estimated by examining the dependence of the coupling integral $F(I_b, p_j)$ according to (6) on the laser beam radius R_b and window position R_w. For that purpose (6) was solved numerically for different sets of R_b and R_w and azimuthal mode excitation. To check the validity of these values, the coupling integral was calculated for radial modes ($R_w = 0$) and for ideal coupling as well, and compared with the theoretical predictions. The results are summarized in Table 3. For ideal coupling, the numerical procedure gives K_j-factors in very good agreement with the theoretical value 1. For radial mode excitation, agreement with theoretical predictions following [15] is also obtained. Figure 3 shows K_j as a function of the window position R_w at constant beam radius R_b and as a function of beam radius at constant window position for azimuthal mode excitation. As can be seen from Fig. 3, K_j is almost independent of the beam radius with only slight increase in K_j by decreasing the

Table 3. Coupling parameter K_j for different beam profiles and types of excited modes; additionally, theoretical predictions for radial mode excitation [15] and ideal beam coupling [16] are given

Spatial intensity distribution I_b	Normal mode p_j	K_j (Computation)	K_j (Theory)
$I_b \sim p_j$, ideal coupling	(100)	0.999	1
	(200)	0.999	1
	(010)	0.998	1
Gaussian distribution according to (5)	(100)[a]	0.479	
	(200)[a]	0.470	
	(010)	0.998	~ 1
	(020)	0.997	~ 1

[a] Reported K_j-values correspond to $R_w = 0.72R$ and $R_b = 0.1R$.

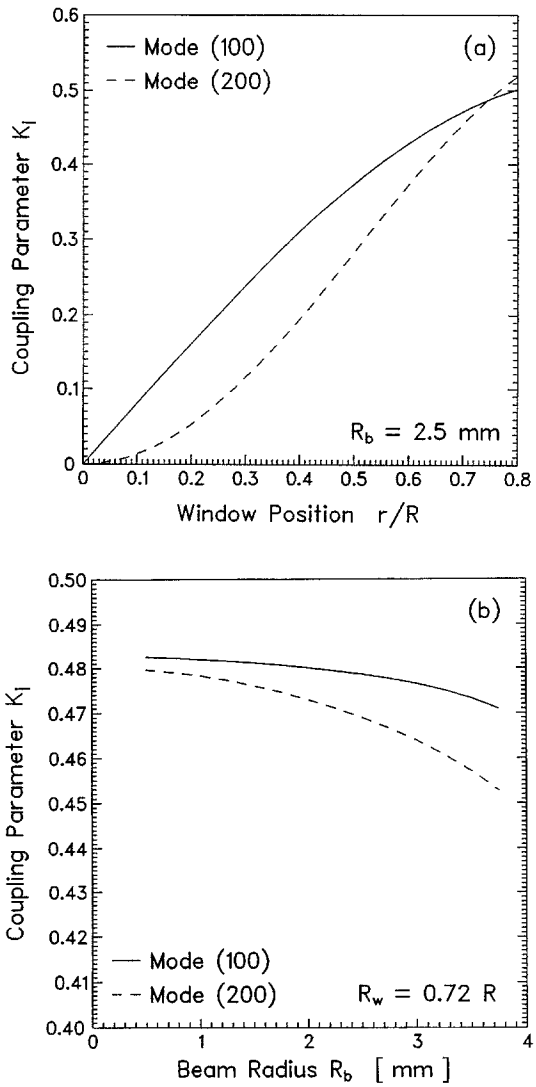

Fig. 3a, b. Coupling parameter K_j as a function of the relative window position r/R at constant beam radius R_b (**a**) and as a function of beam radius R_b at constant window position R_w (**b**) for the excitation of azimuthal modes (m00)

beam radius. A strong but expected dependence of K_j is found on the window position [9].

An important result of this discussion is that for azimuthal mode excitation a K_j-value of 1 is out of reach. The behaviour of K_j in the case of azimuthal mode excitation may be illustrated by the quite different spatial distributions of I_b and p_j. In contrast to the radial mode excitation ($K_j \approx 1$) where both I_b and p_j show a rotational symmetry with respect to the optical axis, I_b and p_j have no common axis of symmetry in the case of azimuthal mode excitation.

4.2 Cell constants

To obtain an estimate of the cell constant for a given resonant cavity, the Q-values following (11), (17), (20)–(22), the K_j-factor taken from Fig. 3, and the normalization factor $P_j J_m$ ($\pi\alpha_{mn}$) taken from Table 1 may be used to calculate C_c from (8). The cavity parameters R and L determine the resonance frequency f_j. The microphone sensitivity S_{micro} has to be derived from a calibration measurement. In our case, we found $S_{micro} = 46$ mV/Pa [13]. Using numerical values summarized in Table 4 we found a quality factor $Q \approx 278$ for excitation of the 2nd azimuthal mode at a resonance frequency of 6700 Hz. The contributions of the different loss mechanisms to the quality factor are:

Free space losses 0.3%
Particle-related relaxational losses 3.1%
Viscous surface losses 68.0%
Thermal surface losses 28.5%
Microphone losses 0.1%

Surface losses are limiting the quality factor, as expected, while losses due to microphone absorption, particle-related relaxational processes and free space dissipation are of minor importance. However, particle-related processes make up the main part of free space losses.

Beside this theoretical approach to a Q-value determination, we used the built-in earphone to measure the Q-value of the resonant cavity by scanning the excitation frequency of the earphone across a normal mode of the cavity to get a more realistic quality factor for the calculation of C_c [13]. These measurements gave $Q \approx 298$ in fairly good agreement with the theoretical value mentioned above. Thus, all important loss mechanisms seem to be considered adequately.

At last, experimental C_c-values were obtained from calibration measurements with spark-discharge generated soot [13]. The results of these measurements are plotted in Fig. 4. Linear regression analysis gave the coefficients $y = 8.9(\pm 0.2)x + 5(\pm 12)$ with the correlation coefficient $r = 0.974$ for mode (100) and $y = 8.9(\pm 0.5)x - 4(\pm 30)$ with $r = 0.987$ for mode (200), respectively. x is the BC mass concentration in $\mu g/m^3$ and y is the photoacoustic signal in μV. A remarkable feature is the low standard deviation of data points corresponding to the mode (200) with respect to those corresponding to the mode (100). If C_c describes the cell response at unit absorbance β and unit power P, the cell constant may be derived from the slope m of the regression line following

$$C_c = \frac{m}{P\sigma_{abs}}. \tag{25}$$

The results of these different approaches to the determination of cell constant C_c are given in Table 5 using numerical values summarized in Table 4 for the calculation of Q.

Table 4. Numerical values used for the calculation of Q acording to (11), (17), and (20)–(22); if not stated otherwise values are given for air [24]

Physical constant	Symbol	Numerical value
Speed of sound	c_0	343 m/s
Density	ρ	1.29 kg/m^3
	ρ_{part} (BC) [25]	1600 kg/m^3
Specific heat	c_p	1005 J/(kg K)
	c_{part} (BC)	716 J/(kg K)
Dynamic viscosity	μ/ρ	1.41×10^{-5} m^2/s
Adiabatic power	γ	1.4
Thermal diffusivity	κ	2.1×10^{-5} m^2/s
Particle diameter	D_p	5.0×10^{-8} m
Mass absorption coefficient	σ_{abs} (BC) [12]	3.0 m^2/g
Roughness of chamber surface	d_{rms} (brass)	3.0×10^{-5} m
Microphone sensitivity	S_{micro}	4.6×10^{-2} V/Pa
Preamplifier gain		$\times 100$
Area of microphone opening	A_{micro}	1.96×10^{-7} m^2
Chamber surface area	S_c	1.96×10^{-2} m^2

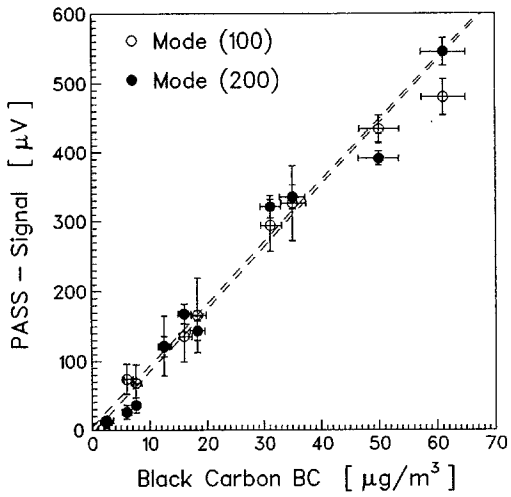

Fig. 4. Calibration measurements with spark-discharge generated black carbon particles

Table 5. Quality factors and cell constants derived from theory, calculated with experimentally obtained Q-values, and derived from BC calibration experiment for azimuthal modes (100) and (200), respectively

	Theory		Theory with exp. Q-values		Calibration	
	(100)	(200)	(100)	(200)	(100)	(200)
Q_j	331	278	305	298	293	330
C_c [V m/W]	5.0	5.5	4.6	5.8	5.9	5.9
C_c [Pa m/W]	1.1	1.2	1.0	1.3	1.3	1.3

The values of $P_j J_m(\pi\alpha_{m0})$ and K_j are 1.7 and 0.479 for mode (100), and 1.87 and 0.470 for mode (200), respectively. A remarkable result is the very good agreement between C_c-values obtained by theory using experimental Q-values and C_c-values derived from calibration measurements. Thus, if a spectrophone is equipped with a built-in earphone or any other device to generate an acoustic test signal a simple method for an absolute calibration may be proposed:

(*i*) Determine the quality factor Q_j of the resonator by mode excitation via the sound source and microphone sensitivity via calibration measurements.
(*ii*) Calculate values of $P_j J_m(\pi\alpha_{m0})$ and K_j according to the equations given above.
(*iii*) Introduce values of Q, $P_j J_m(\pi\alpha_{m0})$, K_j, S_{micro}, and R into (8) and calculate C_c.

Knowing optical power P, either σ_{abs} of the absorbing matter or the spectrophone sensitivity m may be calculated from (25). Applying this procedure to BC as absorbing matter with $P = 0.5$ W and $m = 8.9$ V/(g m^{-3}) [13] a mass absorption coefficient $\sigma_{\text{abs}} = 3.1$ m^2/g is obtained in very good agreement with the theoretical and experimental values for σ_{abs} [12].

4.3 Noise reduction

The improvement in noise reduction with respect to the above-mentioned data processing algorithm was derived from fluctuations of the background signal originating from window heating and sample flow, respectively, and from signal fluctuations at a given BC concentration which also include variations of the soot generator output. The results are summarized in Table 6. Thus, taking the maximum of the fitted profile instead of the maximum signal of a single scan results in an improvement of SNR by a factor of 5. Combining this noise reduction with enhanced noise damping by operation at a higher modulation frequency [13], an overall improvement of SNR by a factor of 10 is achieved when measurements are performed at the 2nd azimuthal mode with peak-height estimation (FIT) instead of a direct measurement of peak height (MAX) at the 1st azimuthal mode.

Finally, based on a background signal fluctuation of 1.4 μV and a sensor sensitivity of 8.9 μV/(μg m^{-3}) the limit of detection is lowered from 4.5×10^{-8} cm^{-1} [13] to 1.5×10^{-8} cm^{-1} or 0.5 μg/m^3 when the proposed data processing algorithm is applied.

Table 6. Mean fluctuation of the background signal BGD (particle-free air) and signal SIG at constant BC mass concentration; MAX labels values corresponding to direct peak height determination, FIT labels values obtained from peak height estimation

		1st azimuthal mode		2nd azimuthal mode	
		MAX	FIT	MAX	FIT
σ_{BGD}	[μV]	12.0	2.3	10.1	1.4
σ_{SIG}	[μV]	36.2	7.9	15.0	3.6

5 Conclusion

A theoretical treatment of an azimuthal resonant spectrophone is given which also includes particle-related relaxational losses as well as the effects of laser beam collimation and window position on the cell constant of the resonator. Based on the excellent agreement between cell constants derived from theory and experiment, a simple method for an absolute calibration of a photoacoustic spectrophone is proposed. The application of this calibration method to particulate carbon as radiation absorbing matter yields a mass absorption coefficient $\sigma_{\text{abs}} = 3.1$ m^2/g for BC at a wavelength $\lambda = 0.802$ μm in good agreement with other experimental findings and theory.

A novel data processing algorithm including a weighted least-squares estimation of the photoacoustic signal is described. In combination with an operation of the spectrophone at the 2nd azimuthal mode this data processing algorithm results in an overall improvement of SNR by a factor of 10. The detection limit of the PASS is lowered to 1.5×10^{-8} cm^{-1} or 0.5 μg BC/m^3 and makes this sensor applicable to measurements of BC mass concentrations in ambient air.

References

1. C.F. Bohren, D.R. Huffman: *Absorption and Scattering of Light by Small Particles* (Wiley, New York 1983)
2. H. Rosen, T. Novakov: Appl. Opt. **22**, 1265 (1983)
3. C.-I. Lin, M. Baker, R.J. Charlson: Appl. Opt. **12**, 1356 (1973)
4. A.D.A. Hansen, H. Rosen, T. Novakov: Sci. Total Environ. **36**, 191 (1984)
5. R.G. Delumyea, L.-C. Chu, E.D. Macias: Atmos. Environ. **14**, 647 (1980)
6. C. Liousse, H. Cachier, S.G. Jennings: Atmos. Environ. **27A**, 1203 (1993)
7. A. Petzold, R. Niessner: Mikrochim. Acta **117**, 215 (1995)
8. A. Rosencwaig: *Photoacoustics and Photoacoustic Spectroscopy* (Wiley, New York 1980)
9. K.M. Adams: Appl. Opt. **27**, 4052 (1988)
10. H. Moosmüller, W.P. Arnott, C.F. Rogers: J. Air Waste Manage. Assoc. (submitted)
11. M.W. Sigrist (ed.): *Air Monitoring by Spectroscopic Techniques* (Wiley, New York 1994)
12. A. Petzold, R. Niessner: SPIE Proc. Soc. Opt. Eng. **1716**, 510 (1992)
13. A. Petzold, R. Niessner: Appl. Phys. Lett. **66**, 1285 (1995)
14. R.W. Terhune, J.E. Anderson: Opt. Lett. **1**, 70 (1977)
15. R.D. Kamm: J. Appl. Phys. **47**, 3550 (1976)
16. C.F. Dewey, Jr.: in *Optoacoustic Spectroscopy and Detection*, ed. by Y.-H. Pao (Academic, New York 1977)
17. A. Karbach, P. Hess: J. Chem. Phys. **83**, 1075 (1985)
18. A. Miklós, A. Lörincz: Appl. Phys. B **48**, 213 (1989)
19. P.M. Morse, K.U. Ingard: *Theoretical Acoustics* (McGraw-Hill, New York 1968)
20. M.R. Da Silva: Can. J. Phys. **64**, 1098 (1986)
21. C.H. Chan: Appl. Phys. Lett. **26**, 628 (1975)
22. P. Gans: *Data Fitting in the Chemical Sciences* (Wiley, New York 1992)
23. P.E. Poston, J.M. Harris: Anal. Chem. **59**, 1620 (1987)
24. R.C. Weast (ed.): *CRC Handbook of Chemistry and Physics* (CRC-Press, Boca Raton, FL 1983)
25. L.W. Richards, R.W. Bergstrom Jr., T.P. Ackerman: Atmos. Environ. **20**, 387 (1986)